

Biophysical Journal

Supporting Material

Confinement Regulates Complex Biochemical Networks: Initiation of Blood Clotting by "Diffusion Acting"

Feng Shen, Rebecca R Pompano, Christian J Kastrup, and Rustem F Ismagilov

SUPPORTING MATERIAL FOR

Confinement Regulates Complex Biochemical Networks: Initiation of Blood Clotting by “Diffusion Acting”

Feng Shen, Rebecca R. Pompano, Christian J. Kastrup, and Rustem F. Ismagilov*

Department of Chemistry and Institute for Biophysical Dynamics, The University of Chicago, 929 East 57th Street, Chicago, Illinois 60637

This document contains

- 1) Materials and Methods
- 2) Supplemental Tables, Figures, and Legends
- 3) Supplemental Text

Materials and Methods

All solvents and salts purchased from commercial sources were used as received unless otherwise stated.

Chemicals and materials

Poly (dimethylsiloxane) (PDMS) (Sylgard Brand 184 Silicone Elastomer kit) and high vacuum grease (silica grease) were purchased from Dow-Corning (Midland, MI). 1,2-dilauroyl-sn-glycero-3-phosphocholine (DLPC), L- α -phosphatidylserine from porcine brain (PS), and L- α -phosphatidylcholine (Egg PC) were purchased from Avanti Polar Lipids (Alabaster, AL). Texas Red® 1,2-dihexadecanoyl-sn-glycero-3-phosphoethanolamine (Texas Red® DHPE) and bis-(p-tosyl-Gly-Pro-Arg amide)-Rhodamine 110 were purchased from Molecular Probes/Invitrogen (Eugene, OR). Normal pooled plasma (human) was purchased from George King Bio-Medical, Inc (Overland Park, KS). t-butylloxycarbonyl- β -benzyl-L-aspartyl-L-prolyl-L-arginine-4-methylcoumaryl-7-amide (Boc-Asp(OBzl)-Pro-Arg-MCA) was purchased from Peptides International (Louisville, KY). Human recombinant tissue factor (TF) was purchased from Calbiochem/EMB Biosciences (La Jolla, CA). Corn trypsin inhibitor was purchased from Haematologic Technologies (Essex Junction, VT). Agarose type IX, pluronic F-68 and silicone isolator (9 mm diameter, 1 mm height) were purchased from Sigma-Aldrich (St. Louis, MO). Biomag® amine magnetic particles (1.5 μ m diameter) were purchased from Bangs Laboratories, Inc. (Fishers, IN). Silica-modified magnetic beads (5 μ m diameter) were purchased from Bioclone, Inc (San Diego, CA). LB growth media was purchased from Difco (Sparks, MD). FEP tubing (1/32 inch outer diameter) was purchased from Upchurch Scientific (Oak Harbor, WA). Plastic syringes (1 mL) were purchased from Becton Dickson (Franklin Lakes, NJ). Pluronic F127 surfactant was purchased from BASF (Mt. Olive, NJ). Chloramphenicol was purchased from Fisher Scientific (Pittsburgh, PA). Krytox®, a fluorinated grease, was purchased from Dupont (Wilmington, DE). Plastic coverslips for microfluidic chambers were purchased from Hampton Research (Aliso Viejo, CA)

Preparing bacterial samples

Bacillus cereus (*B. cereus*) GFP was *B. cereus* UW85 43-25 (source, J. Handelsman, Univ. of Wisconsin). Bacteria were grown on Luria-Bertani (LB) plates at 37° C for ~ 14 h. Chloramphenicol was used as the antibiotic in the culture media. The bacteria were then localized in gel microdroplets (GMDs) (1,2) to create “bacteria GMDs”. To do so, bacteria were concentrated by centrifugation at 10,000 rpm for 10 min, and then the supernatant was removed. An agarose solution was prepared containing 20 mg agarose IX, pluronic F-68 (20 µL of a 10% solution), Biomag® amine magnetic particles (1.5 µm diameter, 100 µL of a solution at 50 mg/mL), and liquid LB growth media (400 µL). This solution was melted by heating to 90° C, then allowed to cool in a 37° C oven. Next, 500 µL of this solution was added to a microcentrifuge tube containing bacteria. The combined solution was separated into droplets ~50 µm in diameter by using a microfluidic approach (3), and the droplets were cooled to 4° C to solidify the agarose.

Preparing TF-carrying beads

Lipid vesicles were prepared as previously described (4). TF was reconstituted into lipid vesicles of 79.5 mol % of DLPC, 20 mol % of PS, and 0.5 mol % of Texas Red DHPE at a lipid concentration of 1.25 mg/mL. The final concentration of TF in the vesicles solution was 8 pM (TF:lipid ratio of 5×10^{-9}). Silica-modified magnetic beads or bead clusters (9-11 µm diameter) were mixed with vesicles containing TF to create TF-coated magnetic silica microparticles (“TF-carrying beads”). After 20 min of incubation at room temperature, the beads were rinsed with saline solution (150 mM NaCl solution) three times. All beads were used within 3 h of preparation.

Measuring clot times of plasma

Normal pooled human plasma (citrate and platelet-poor) was purchased frozen and stored at -80°C. Before use, plasma samples were thawed at room temperature and then incubated with corn trypsin inhibitor (100 µg/mL) to inhibit the factor XII pathway of initiation of coagulation. Plasma was recalcified in 300 µL aliquots by adding 100 µL of a solution of 40 mM CaCl₂, 90 mM NaCl, 50 µM ZnCl₂ and 0.4 mM of a thrombin-sensitive fluorescent substrate, either Boc-Asp(OBzl)-Pro-Arg-MCA or bis-(p-tosyl-Gly-Pro-Arg amide)-Rhodamine 110. In all experiments, clot times were determined by monitoring the formation of thrombin and fibrin. In experiments using bacteria GMDs, the formation of thrombin was monitored by fluorescence microscopy to detect the cleavage products from the thrombin-sensitive fluorescent substrate Boc-Asp(OBzl)-Pro-Arg-MCA, which fluoresces in blue. In experiments using TF-carrying beads, the formation of thrombin was monitored by confocal microscopy to detect the cleavage products from the thrombin-sensitive fluorescent substrate bis-(p-tosyl-Gly-Pro-Arg amide)-Rhodamine 110, which fluoresces in green. The formation of fibrin was detected by using brightfield microscopy. The clot time was defined as the first appearance of fibrin, which always corresponded to the onset of increasing fluorescence due to generation of thrombin.

Preparing devices with plasma and TF-carrying beads or bacteria GMDs

All devices were fabricated by using rapid prototyping in PDMS (5). The devices consisted of channels of different sizes, with cross sections of $160 \times 160 \mu\text{m}^2$, $40 \times 40 \mu\text{m}^2$, and $10 \times 10 \mu\text{m}^2$ (see Figure 1). The devices were sealed by using a Plasma Prep II (SPI Supplies, West Chester, PA), and then they were baked overnight at 110 °C. Next, the devices were placed into a saline

solution (150 mM NaCl) and kept under a vacuum overnight to completely saturate the PDMS. Solutions were flowed into the microfluidic devices through FEP tubing connected to glass or plastic syringes. For handling of blood, the tubing was connected to plastic syringes and the syringes were blocked with a solution containing Pluronic F127 surfactant prill (0.2% in phosphate buffered saline). Prior to adding the bacteria GMDs or blood, the microfluidic channels were coated with inert phospholipids by flowing vesicles of L- α -phosphatidylcholine (Egg PC) (1.25 mg mL⁻¹) through the device at a flow rate of 1.0 μ L min⁻¹ for 20 min. Excess vesicles were removed by flowing a solution of saline through the channels for 10 min at a flow rate of 1.0 μ L min⁻¹. For TF experiments, TF-carrying beads in a saline solution (150 mM NaCl) were flowed into the device and either localized in the 160 \times 160 μ m² channel by using magnets or trapped in the 10 \times 10 μ m² channels by fluid flow. Next, plasma was flowed through the device, and then the device was sealed with silica grease to stop flow.

For bacteria experiments, two different experimental setups were used to achieve confined and less confined conditions. To confine bacteria, bacteria GMDs were mixed with plasma first, and then the plasma containing bacteria GMDs was flowed through the device. Bacteria GMDs were trapped in the 40 \times 40 μ m² channels, and then the inlet and outlet openings of the microfluidic devices were sealed with silica grease to stop flow. To create less confined conditions, we used a microfluidic chamber consisting of two plastic coverslips separated by a silicone isolator (9 mm diameter, 1 mm height) coated with an inert fluorinated grease (Krytox®). The bacteria GMDs were placed into the chamber and their position was constrained near the center of bottom in the chamber by using magnets. Plasma was then pipetted in to fill the chamber, and the device was sealed. TF-carrying beads and the bacteria GMDs varied slightly in size. To compensate, we looked at beads or GMDs in the less confined condition that were equal-sized or slightly bigger than those in the more confined condition.

Image acquisition and preparation

The confocal images from experiments using TF-carrying beads were acquired by using a digital camera (C9100, Hamamatsu Photonics, Japan) mounted on a Visitech VT Infinity 3 multi-point confocal system (VisiTech International Ltd., United Kingdom) attached to Leica DMI 6000 B microscope with a 20 \times 0.7 NA objective at room temperature. All the other fluorescence and brightfield images were acquired by using a digital camera (C4742, Hamamatsu Photonics, Japan) mounted to a Leica DMI 6000 B epi-fluorescence microscope with a 10 \times 0.4 NA objective at 37 °C.

Analysis of fluorescence images

Image analysis was performed as previously described (4). The original grayscale fluorescence images were collected and false-colored by using MetaMorph software (Molecular Devices, Sunnyvale, CA). Although the bis-(p-tosyl-Gly-Pro-Arg amide)-Rhodamine 110 dye used for experiments using TF-carrying beads fluoresces in green, its fluorescence was false-colored in blue for clarity in the manuscript. For each wavelength, the intensity levels were adjusted to the same values for all images. Images were overlaid by using adobe Photoshop software (Adobe, San Jose, CA).

Numerical simulation of blood coagulation

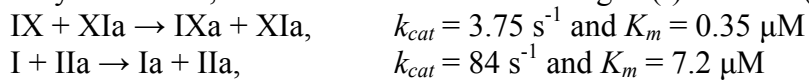
The coagulation network was modeled in Comsol Multiphysics 3.3 and 3.5a by using a previously published numerical model (6) based on the model described by others (7).

Geometry: The model was assembled using a geometry drawn in either 2D (Fig. 3, 6), 2D-axially symmetric space (Fig. 4, 5). 2D-axial symmetry is referred to as “quasi-3D” because this geometry recapitulates the diffusion profile that is obtained in fully 3D simulations. Preliminary simulations confirmed this assumption: For the fully confined geometry drawn in Fig. 4, a 2D-axially symmetric geometry gave essentially the same t_{clot} as a fully 3D geometry. This simulation used a chamber size small enough to permit a 3D simulation to run on the available computer: $R = 28.2 \mu\text{m}$, $r = 25 \mu\text{m}$, and $[\text{TF}] = 5 \text{ pM}$ ($\text{CT} = 533 \text{ s}$). The resulting t_{clot} for 2D-axially symmetric and 3D simulations was 744 and 738 s respectively, whereas for a 2D (no symmetry implemented) simulation it was 660 s. The dimensions used for the various simulations are given in Fig. 3 and Tables S1, S2, and S3.

The 2D rectangular geometry used in Fig. 6 is also referred to as “quasi-3D” because this geometry is equivalent to a slice through a pair of parallel plates that contain a surface patch of infinite length. The chamber consisted of a rectangle of length 10.5 mm and height R (10 or 100 μm). The patch consisted of a rectangle of length 200 μm and height 1 μm . The bottom of the patch was aligned with the bottom of the chamber, centered 0.5 mm from the left edge of the chamber.

Units used in numerical simulation: For 2-dimensional (2D) simulations, Comsol Multiphysics accepts volume concentrations (mol/m^3) instead of surface concentrations (mol/m^2), by calculating total quantities in mol/m to make the depth in the z-direction irrelevant. For example, a 6 μm circular patch of TF in 2D (surface area $3 \times 10^{-23} \text{ m}^2$) with $[\text{TF}] = 1 \text{ nM}$ ($1 \times 10^{-6} \text{ mol}/\text{m}^3$) has total quantity Surface Area \times Concentration = $3 \times 10^{-29} \text{ mol}/\text{m}$.

Kinetics: This model used 45 species interacting via 40 rate equations that describe enzyme kinetics and stoichiometric inhibition in blood coagulation, without surface interactions (6, 7). The simulations for the current work also included two additional reactions (8): the activation of factor IX by factor XIa, and the conversion of fibrinogen (I) to fibrin (Ia) by thrombin (IIa).



The rates of these two reactions were described by Michaelis-Menten rate equations, i.e. for the former reaction, $\text{Rate} [\mu\text{M}/\text{s}] = k_{cat} \times [\text{XIa}] \times [\text{IX}] / (K_m + [\text{IX}])$, and similarly for the latter reaction. The initial concentration of fibrinogen was 8.3 μM . The initial concentrations of activated factors XIa, Xa, IXa, VIIIa, Va, IIa (α -thrombin), and mIIa (meizothrombin) were set to 1 femtomolar (1 fM) to better replicate standard clotting responses. TF, TF complexes, and fibrin did not diffuse ($D = 0 \text{ m}^2/\text{s}$), and all other species had the same diffusion coefficient, $D = 5 \times 10^{-11} \text{ m}^2/\text{s}$.

Fluid flow: Fluid flow was modeled in Fig. 6 using fluid density = 1000 kg/m^3 and viscosity = 0.0015 Pa s. The initial fluid velocity throughout all subdomains was given by $U_{avg} = (1/6) \times (\text{shear rate}) \times R$, where the shear rate was 1 s^{-1} and R is the height of the chamber. U_{avg} was

1.67×10^{-6} and 1.67×10^{-5} m/s for $R = 10$ and $100 \mu\text{m}$, respectively. No-slip boundary conditions were used for the top and bottom walls of the chamber. The left boundary of the chamber was an inlet, with inflow velocity $U_0 = U_{avg} \times 6 \times s \times (1 - s)$, where s is a boundary variable that goes linearly from 0 to 1 along the length of the boundary. The right boundary was an outlet, with gauge pressure = 0. This model was solved to obtain a steady-state parabolic flow profile, which had maximum velocity $U_{max} = 1.5 \times U_{avg}$, as expected for flow between parallel plates. The steady-state flow profile was then used for calculating the convection of reactive species in the Convection-Diffusion module.

Mesh: Each simulation was meshed to obtain reasonable spatial resolution, using a Free (triangular) mesh. For simulations in Fig. 4, preliminary simulations comparing Normal and Finer mesh yielded similar values of t_{clot} .

Fig. 3 (2D microfluidic geometry): Meshed with Coarser mesh, modified by constraining the edge element distribution along the edges of the $10 \mu\text{m}$ -wide channels to (0: 1/200 : 1), to obtain regularly spaced mesh vertices roughly as far apart as the width of the channel.

Fig. 4 and 5 (quasi-3D confinement): Meshed with default Normal mesh.

Fig. 6 (quasi-3D confinement): Meshed with Extremely Fine mesh, modified to reduce the number of elements near the $1 \mu\text{m}$ tall patch while maintaining spatial resolution across the channel. For the large chamber ($R = 100 \mu\text{m}$), Maximum element scaling factor = 0.08, Element growth rate = 1.2, Resolution of narrow regions = 0.25. For the small chamber ($R = 10 \mu\text{m}$), Maximum element scaling factor = 0.02, Element growth rate = 1.25, Resolution of narrow regions = 0.25, plus one Refinement was done of the mesh in the chamber domain over the patch.

Solver settings: A Convection/Diffusion module was used to model reaction and diffusion processes, using a Transient, Time-dependent solver (Geometric Multigrid or PARDISO) with Free time-stepping (i.e. time steps for calculation were chosen by the solver). Absolute error tolerance was $1e-9$ (Fig. 4) or $1e-12$ (Fig. 3, 5, 6). Relative error tolerance was 0.01 in all cases. For Fig. 6, fluid flow was modeled using a Navier-Stokes module, using a Steady-state, stationary solver (PARDISO).

Determining C_{crit} for the simulated coagulation network

To identify the critical concentration of thrombin, C_{crit} [μM], for the simulated coagulation cascade, the simulation was initiated in the presence of varying initial concentrations of free α -thrombin, $[\text{IIa}]_0$, to find the lowest $[\text{IIa}]_0$ that could initiate clotting. A spatially homogeneous geometry without TF was used, and the clot time was defined as the time at which fibrin reached half of its maximum concentration (i.e., at $4.15 \mu\text{M}$ fibrin). For $[\text{IIa}]_0 \leq 22 \text{ pM}$, clotting was not initiated within 500 min, while for $[\text{IIa}]_0 \geq 23 \text{ pM}$ clotting was initiated in 86 min or less. For simplicity, the concentration of free α -thrombin, $[\text{IIa}]$, was converted into a quantity that is easier to observe experimentally, the concentration of free α -thrombin plus free meizothrombin ($[\text{IIa} + \text{mIIa}]$). We tested whether 23 pM IIa corresponded to a particular $[\text{IIa} + \text{mIIa}]$ during simulations of TF-initiated clotting. For simulated clotting initiated with 5 – 20 pM TF, we found the time at which $[\text{IIa}]$ reached 23 pM and recorded $[\text{IIa} + \text{mIIa}]$ at this time. This showed that 23 pM IIa

corresponded to $[IIa + mIIa] \sim 10.6$ nM. In experiments, fibrin usually forms when $[IIa + mIIa]$ is ~ 10 nM (9). Based on these results, we defined C_{crit} in this work as 10.6 nM $IIa + mIIa$.

Testing Eq. 1 for blood coagulation

For simulations to test Eq. 1 (see Results), each parameter in the equation was systematically varied. R and r were varied by changing the size of the chamber or the patch, respectively, using constant $[TF] = 20$ pM. CT (defined in Results) was varied by changing $[TF]$ on the patch (5, 10, 15, or 20 pM), using constant $R = 84.6$ μm and $r = 33$ μm . CT was determined for each $[TF]$ by using a uniform system having $R = r = 25$ μm . t_{clot} was defined as the time when the average $[IIa + mIIa]$ reached C_{crit} . At this time, the concentration at center of the patch was also equal to C_{crit} because the thrombin was essentially uniformly distributed throughout the chamber on the timescale of clotting (Fig. S3).

Supplemental Figures and Tables

Figure S1. Bright field microscopy was used to monitor fibrin formation. No fibrin formed in a channel with 10×10 μm^2 cross-section in the absence of Tissue Factor (TF)-carrying bead (top channel); Fibrin mesh formed when TF-carrying bead was confined in a channel with a 10×10 μm^2 cross-section (bottom channel).

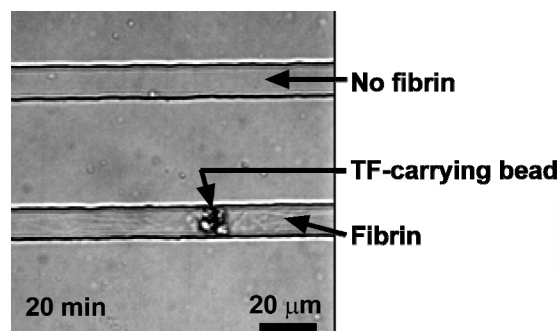


Table S1. To test whether Eq. 1 holds for blood coagulation, a quasi-3-dimensional numerical simulation was conducted using a quasi-spherical patch of TF in a quasi-spherical chamber of plasma, systematically varying each of the three terms in the equation, $t_{clot} = CT \times R^3/r^3$: chamber radius R , patch radius r , and clot time of a uniform system CT .

$[TF]_0$, pM	CT , s	R , μm	r , μm	R^3/r^3	t_{clot} , s	t_{clot}/CT
5	533	84.6	33	16.85	15657	29.38
10	286	84.6	33	16.85	3673	12.84
15	196	84.6	33	16.85	2462	12.56
20	152	84.6	33	16.85	1904	12.53
20	152	28.2	25	1.44	207	1.36
20	152	84.6	50	4.84	637	4.19
20	152	55	25	10.65	1276	8.39
20	152	70	25	21.95	2428	15.97
20	152	84.6	27	30.76	3292	21.66
20	152	84.6	25	38.75	4220	27.76

The plot of t_{clot}/CT versus R^3/r^3 fell on a line of slope 0.699 ± 0.008 (goodness of fit = 0.999).

Table S2. To test whether Eq. 1 holds for blood coagulation, a 2-dimensional numerical simulation was conducted using a circular patch of TF in a circular chamber of plasma, systematically varying each of the three terms in the equation $t_{clot} = CT \times R^2/r^2$: chamber radius R , patch radius r , and clot time of a uniform system CT .

$[TF]_0$, pM	CT , s	R , μm	r , μm	R^2/r^2	t_{clot} , s	t_{clot}/CT
5	540	84.6	35	5.84	2527	4.68
10	287	84.6	35	5.84	1360	4.74
15	196	84.6	35	5.84	967	4.93
20	152	84.6	35	5.84	736	4.84
5	540	84.6	84.6	1.00	540	1.00
5	540	84.6	80	1.12	591	1.09
5	540	28.2	25	1.27	661	1.22
5	540	84.6	50	2.86	1339	2.48
5	540	56.4	25	5.09	2271	4.21
5	540	84.6	35	5.84	2527	4.68
5	540	70	25	7.84	3394	6.29
5	540	84.6	30	7.95	3392	6.28
5	540	84.6	25	11.45	5274	9.77

The plot of t_{clot}/CT versus R^2/r^2 fell on a line of slope 0.81 ± 0.02 (goodness of fit = 0.998).

Figure S2. 2-dimensional numerical simulations of a patch of TF of radius r centered in a chamber of plasma of radius R showed that the observed time to reach the critical concentration of free thrombin plus meizothrombin (t_{clot}) scaled linearly with R^2/r^2 and with CT , as predicted by Eq. 1. The 2D geometry is drawn schematically at the left.

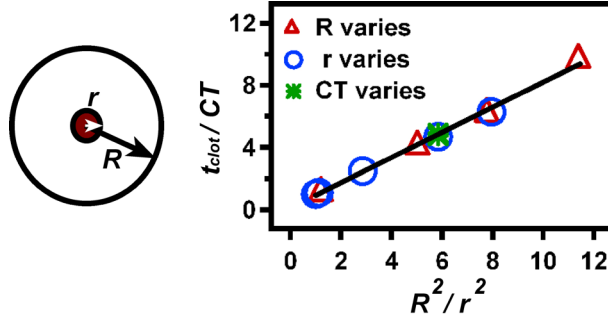
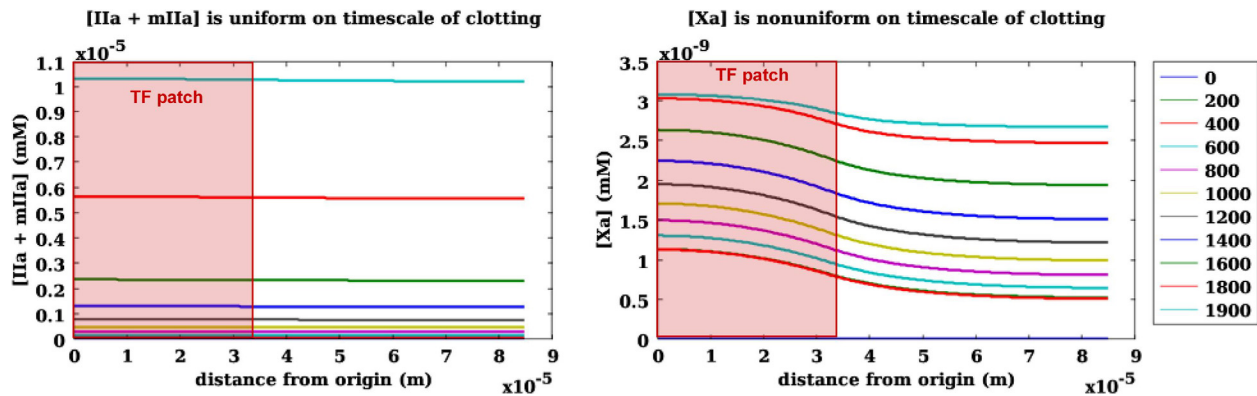


Table S3. To test whether Da_2 could accurately predict the outcome of sub-threshold patches of stimulus in open chambers of plasma, a quasi-3-dimensional numerical simulation was conducted using a cylindrical patch of TF in a cylindrical chamber of plasma, systematically varying the chamber radius R , and patch radius r . The clot time of uniform system, CT , was held constant at 152 s by using $[TF] = 20$ pM. Simulations that did not clot within 30,000 s (8.3 hr) were considered unclotted.

$r, \mu\text{m}$	$R, \mu\text{m}$	R^2/r^2	Cn	Da_2	t_{clot}, s	t_{clot}/CT
25	25	1.00	0.0000	4.112	154	1.01
25	35	1.96	0.0016	2.091	305	2.01
15	25	2.78	0.0016	1.477	436	2.87
25	50	4.00	0.0100	1.018	640	4.21
25	55	4.84	0.0144	0.839	773	5.09
7	19	7.37	0.0023	0.557	1280	8.42
8	25	9.77	0.0046	0.420	1700	11.18
7	25	12.8	0.0052	0.322	2257	14.85
6	25	17.4	0.0058	0.237	3206	21.09
6	28	21.8	0.0077	0.189	4617	30.38
5	25	25.0	0.0064	0.164	6254	41.14
8	42	27.6	0.0185	0.149	7968	52.42
8	43	28.9	0.0196	0.142	> 30000	> 197.37
4	23	33.1	0.0058	0.124	> 30000	> 197.37
4	25	39.1	0.0071	0.105	> 30000	> 197.37
3	25	69.4	0.0077	0.059	> 30000	> 197.37

Figure S3. Thrombin is uniformly distributed on the timescale of clotting and factor Xa is not. A quasi-3-dimensional numerical simulation of coagulation was conducted for a quasi-spherical chamber with radius $R = 84.6 \mu\text{m}$ containing a patch of 20 pM TF with radius $r = 33 \mu\text{m}$. Linescans of concentration taken from the center of the patch (*origin*) to the wall were plotted for a series of time points leading up to $t_{clot} = 1904 \text{ s}$. The location of the TF patch is shown in red shading on the plots. (left) Linescans of the concentration of thrombin plus meizothrombin, $[\text{IIa} + \text{mIIa}]$ were flat, indicating uniformity of the distribution across the chamber. The total deviation of $[\text{IIa} + \text{mIIa}]$ at time t_{clot} is $< 1.0 \%$ of the average concentration at that time. Thus coagulation initiates simultaneously throughout the chamber, not just at the center of the patch. See also supplemental text, below. (right) Linescans of the concentration of factor Xa, $[\text{Xa}]$, showed non-uniformity of the distribution across the chamber. The total deviation of $[\text{Xa}]$ at time t_{clot} is 15% of the average concentration at that time.



Supplemental Text

Coagulation in simulated microfluidic device

As stated in the main text, a patch of TF in the confining ($10 \mu\text{m}$) channels initiated the simulated coagulation network quickly (7.6 min). In the less confining ($160 \mu\text{m}$) channel connected to the confining channels as drawn in Figure 3, coagulation occurred more slowly (35.9 min) due to propagation of the clot from the smaller to the larger channel. To confirm that this coagulation was due only to propagation and not to initiation by the TF patch in the large channel, a control simulation was conducted with a patch of TF in an isolated $160 \mu\text{m}$ channel. Coagulation did not occur in 60 min , the duration of the simulation.

Discussion of Eq. (1), $t_{clot} = CT \times V_c/V_p$

Average distance diffusing thrombin travels in 1 minute:

The distance x traveled by the average thrombin molecule in time t is given by

$$x = (2n D t)^{0.5}, \quad \text{where } n = \text{number of dimensions (i.e. 1, 2, or 3)}$$

Using diffusion coefficient $D = 5 \times 10^{-11} \text{ m}^2/\text{s}$ (as in previous work (6)), $t = 60 \text{ s}$, x is

n	x
1	77 μm
2	110 μm
3	134 μm

Diffusion inside of a blood vessel or atop a surface patch can usually be described as occurring in 2 or 3 dimensions, so this calculation shows that thrombin diffuses on the order of 100 $\mu\text{m}/\text{min}$. This is used to justify the approximation that diffusion in small chambers occurs rapidly relative to coagulation, which usually requires > 2 minutes.

Derivation

We define t_{clot} [s] as the time required for a patch of stimulus (TF) to produce enough activator (thrombin) to bring the average concentration in a confined volume up to the critical concentration, C_{crit} . Thus by definition we have

$$(S1) \quad t_{clot} = \frac{(C_{crit} - C_0) \times V_c}{Rate} \quad \text{where } C_{crit} = \text{critical concentration} = 10.6 \text{ nM IIa} + \text{mIIa}$$

C_0 = initial average concentration $\approx 2 \text{ fM IIa} + \text{mIIa}$

V_c = volume of chamber [m^3]

$Rate$ = Net rate of production of IIa + mIIa [mol/s]

Experimentally the clot time is sometimes not observable at t_{clot} , but instead is observed at some later endpoint such as the time at which fibrin forms, corresponding to a concentration of activator C_{obs} , e.g. 10 – 30 nM (9) or ~ 75 -150 nM IIa + mIIa (see comment 3 below). The observed clot time t_{obs} can be described as:

$$(S2) \quad t_{obs} = t_{clot} + \Delta_{clot}$$

where Δ_{clot} = time delay [s] from C_{crit} to C_{obs}
(Comment 3)

Rate is a function of the concentration of stimulus. For a typical clotting experiment, *Rate* is not measured directly, but can be inferred from the time needed to for a uniform system to clot.

$$(S3) \quad Rate = \frac{C_{obs} \times V_p}{CT_{obs}}$$

where C_{obs} = concentration at observed clot time (mIIa +
IIa, nM)

V_p = volume of patch [m³]

$CT_{obs} = t_{obs}$ in a system with uniform stimulus

Using the same treatment for CT_{obs} as in Eq. S2, we obtain

$$(S4) \quad Rate = \frac{C_{obs} \times V_p}{CT + \Delta_{CT}}$$

where $CT = t_{clot}$ in a system with uniform stimulus

Δ_{CT} = time delay [s] from C_{crit} to C_{obs} in a system
with uniform stimulus

Returning to Eq. (S1), we assume that C_0 is negligible compared to C_{crit} , and insert Eq. (S4) into Eq. (S1) to obtain

$$(S5a) \quad t_{clot} = \frac{C_{crit} \times V_c}{C_{obs} \times V_p} \times (CT + \Delta_{CT})$$

$$(S5b) \quad t_{obs} = \frac{C_{crit} \times V_c}{C_{obs} \times V_p} \times (CT + \Delta_{CT}) + \Delta_{clot}$$

Finally, we use the special case when $C_{obs} = C_{crit}$, as it often is in simulations and in some experiments. In this case, $\Delta_{CT} = \Delta_{clot} = 0$, $t_{obs} = t_{clot}$, and Eqs. (S5) both simplify to

$$(S6) \quad t_{clot} = \frac{V_c}{V_p} CT$$

which is the result given in the main text.

Comments

1. This treatment of *Rate* finds the time-averaged net rate of production of activator, from the initial time until t_{obs} , and uses it as a constant net rate. We note that in our simulations of blood coagulation, the rate of production of thrombin is indeed mostly constant during the initiation stage of clotting, and increases nonlinearly only after the critical concentration is reached. Thus, this treatment is most valid when we use $C_{obs} = C_{crit}$.

2. Equation (S6) considers only the average concentration in the chamber at each time point, so the shape and precise location of the patch within the chamber do not play a role in the calculation. This treatment may break down if the patch is located much closer to one wall than another, in which case clotting may occur even faster than predicted.

3. We note that t_{clot} as we have defined it may not be easily observed in clotting blood in all experiments, as its observation requires continuous monitoring of the thrombin concentration and a reasonable estimate of C_{crit} . The clot time that is easily observed, t_{obs} , may occur later, such as when fibrin becomes visible or the blood reaches a particular opacity or stiffness. At this time, the activator has reached a concentration C_{obs} ($C_{obs} \geq C_{crit}$). In this case, equation (S5b) should be used to describe the scaling of the clot time of the system under confinement. We did not explore this case in detail in this work, but we observed in numerical simulations that Δ depends slightly on the concentration of TF. For example, setting t_{obs} as time to reach half-maximum fibrin formation (4.15 μ M Ia), and t_{clot} as the time to reach 10.6 nM IIa+mIIa, for a uniform system with [TF] = 5, 10, 15, and 20 pM we found Δ_{CT} = 182, 157, 146, and 132 s, respectively. Interestingly, comparing Δ_{CT} to the data for CT in Table S1, we found that Δ_{CT} is much less dependent on [TF] than CT is. We also noted that with this setting for t_{obs} , C_{obs} was \sim 75 - 150 nM [IIa + mIIa], which is on the order of 10-fold larger than C_{crit} . For example, for [TF] = 5 pM in a uniform system, C_{obs} was 120 nM [IIa + mIIa]; C_{obs} increases for greater [TF] and decreases for greater R^2/r^2 , even though C_{crit} remains unchanged by definition.

Discussion of dimensionality for Da_2

Cn and Da_2 contain the terms n_w and n_f , and the number of dimensions that are enclosed by a wall or not enclosed by a wall, respectively. These values are straightforward to obtain for symmetric systems such as spherical chambers ($n_w = 3$, $n_f = 0$), and for open-ended chambers such as open cylinders ($n_w = 2$, $n_f = 1$). Interpretation is possible for other geometries, such as a closed chamber with a large aspect ratio. For example, a long cylindrical chamber with closed ends technically has $n_w = 3$ and $n_f = 0$, which gives $Da_2 = \text{infinity}$. However, one can use $n_w = 2$ and $n_f = 1$ to determine whether the side-walls are sufficient to induce clotting on a more rapid timescale.

References:

1. Weaver, J. C., G. B. Williams, A. Klibanov and A. L. Demain. 1988. Gel Microdroplets - Rapid Detection and Enumeration of Individual Microorganisms by Their Metabolic-Activity. *Bio-Technology*. 6:1084-1089.
2. Zengler, K., G. Toledo, M. Rappe, J. Elkins, E. J. Mathur, J. M. Short and M. Keller. 2002. Cultivating the uncultured. *Proc. Natl. Acad. Sci. U. S. A.* 99:15681-15686.
3. Zhang, H., E. Tumarkin, R. Peerani, Z. Nie, R. M. A. Sullan, G. C. Walker and E. Kumacheva. 2006. Microfluidic production of biopolymer microcapsules with controlled morphology. *J. Am. Chem. Soc.* 128:12205-12210.
4. Kastrup, C. J., M. K. Runyon, F. Shen and R. F. Ismagilov. 2006. Modular chemical mechanism predicts spatiotemporal dynamics of initiation in the complex network of hemostasis. *Proc. Natl. Acad. Sci. U. S. A.* 103:15747-15752.
5. Duffy, D. C., J. C. McDonald, O. J. A. Schueller and G. M. Whitesides. 1998. Rapid prototyping of microfluidic systems in poly(dimethylsiloxane). *Anal. Chem.* 70:4974-4984.
6. Kastrup, C. J., J. Q. Boedicker, A. P. Pomerantsev, M. Moayeri, Y. Bian, R. R. Pompano, T. R. Kline, P. Sylvestre, F. Shen, S. H. Leppla, W. Tang and R. F. Ismagilov. 2008. Spatial Localization of Bacteria Controls Coagulation of Human Blood by "Quorum Acting". *Nat. Chem. Biol.* 4:742-750.
7. Hockin, M. F., K. C. Jones, S. J. Everse and K. G. Mann. 2002. A model for the stoichiometric regulation of blood coagulation. *J. Biol. Chem.* 277:18322-18333.
8. Kogan, A. E., D. V. Kardakov and M. A. Khanin. 2001. Analysis of the activated partial thromboplastin time test using mathematical modeling. *Thromb. Res.* 101:299-310.
9. Mann, K. G., K. Brummel and S. Butenas. 2003. What is all that thrombin for? *J. Thromb. Haemost.* 1:1504-1514.